ApJ
Preprint typeset using LaTeX style emulateapj v. 5/2/11

THE SPIN OF THE BLACK HOLE IN THE X-RAY BINARY NOVA MUSCAE 1991

ZIHAN CHEN,[1,2] LIJUN GOU,[1,2] JEFFREY E. MCCLINTOCK,[3] JAMES F. STEINER,[3] JIANFENG WU,[3] WEIWEI XU,[1,2]
JEROME A. OROSZ,[4] YANMEI XIANG[1,5]

ApJ

ABSTRACT

The bright soft X-ray transient Nova Muscae 1991 was intensively observed during its entire 8-month outburst using the Large Area Counter (LAC) onboard the *Ginga* satellite. Recently, we obtained accurate estimates of the mass of the black hole primary, the orbital inclination angle of the system, and the distance. Using these crucial input data and *Ginga* X-ray spectra, we have measured the spin of the black hole using the continuum-fitting method. For four X-ray spectra of extraordinary quality we have determined the dimensionless spin parameter of the black hole to be $a_* = 0.63^{+0.16}_{-0.19}$ (1σ confidence level), a result that we confirm using eleven additional spectra of lower quality. Our spin estimate challenges two published results: It is somewhat higher than the value predicted by a proposed relationship between jet power and spin; and we find that the spin of the black hole is decidedly prograde, not retrograde as has been claimed.

Subject headings: accretion, accretion disks – binaries:individual (GRS 1124–683; GS 1124–683; Nova Muscae 1991) – black hole physics – X-rays:binaries

1. INTRODUCTION

On 1991 January 8, a bright X-ray nova was discovered independently using the *Ginga* and *Granat* X-ray satellites by Kitamoto et al. (1992) and Brandt et al. (1992) who named the source GS 1124–683 and GRS 1124–68, respectively. Located in the constellation Musca, the X-ray source is also known as X-ray Nova Muscae 1991 (hereafter, NovaMus). After the system returned to quiescence, optical observations revealed an orbital period of 10.4 hr and a large mass function (Remillard et al. 1992), which established that the system is one of about a dozen short-period X-ray binaries ($P_{\rm orb} < 12$ hr) whose compact X-ray source is a dynamically-confirmed black hole. The prototype of this subclass of black hole binaries is A0620–00. Other well studied short-period systems include GRO J0422+32, XTE J1118+480, XTE J1859+228 and GS 2000+25.

During the past decade, the spins of many black holes have been estimated using two methods: fitting the profile of the Fe K line (Fabian et al. 1989; Reynolds 2014) and fitting the thermal continuum spectrum (Zhang et al. 1997; McClintock et al. 2014)[6]. It is the continuum-fitting method that we employ here in measuring the spin of NovaMus, and that our group has developed and used to measure the spins of ten stellar-mass black holes (McClintock et al. 2014; Steiner et al. 2014; Gou et al. 2014).

In the continuum-fitting method, the spin of a black hole with known mass and distance is estimated by fitting the thermal component of emission to a corrected version of the thin-disk model of Novikov and Thorne (Li et al. 2005) while employing an advanced treatment of spectral hardening (Davis et al. 2005; Davis & Hubeny 2006). For the successful application of the method, it is essential to consider only those spectra that contain a dominant thermal component (Steiner et al. 2009a) and for which the Eddington-scaled disk luminosity is moderate, $l \equiv L_{\rm bol}(a_*, \dot{M})/L_{\rm Edd} < 0.3$ (McClintock et al. 2006).

The robustness of the continuum-fitting method has been demonstrated by the very many independent and consistent measurements of spin that have been obtained for several black holes (e.g., Steiner et al. 2010); by extensive theoretical studies of the thin-disk model (Shafee et al. 2008; Penna et al. 2010; Noble et al. 2011; Kulkarni et al. 2011; Zhu et al. 2012); and through careful consideration of a wide range of systematic errors (McClintock et al. 2014; and references therein). In applying the method, one must usually make the weakly-tested assumption that the spin of the black hole is closely aligned with the angular momentum vector of the inner disk (Steiner & McClintock 2012; Fragos et al. 2010).

A crucial requirement of the continuum-fitting method is that one have accurate estimates of three system parameters: the black hole mass M, the disk inclination i and the source distance D. Using optical dynamical data of unprecedented quality and published light curves, we have obtained definitive measurements of these parameters for NovaMus: $M = 11.0^{+2.1}_{-1.4}\ M_\odot$, i $= 43.2^{+2.1}_{-2.7}$ deg, $D = 4.95^{+0.69}_{-0.65}$ kpc (Wu et al. 2015b). With the values of these key parameters in hand, in the following sections we fit X-ray data obtained during the 1991 outburst of NovaMus, estimate the spin of its black hole, and present and discuss our results.

We earlier estimated the spin of the black hole in the prototype of the short-period systems, A0620–00, and found it to be exceptionally low $a_* = 0.12 \pm 0.19$ (Gou et al. 2010). Another notable feature of this study of A0620–00 was the extreme dominance of the thermal disk component: The Compton component contributed $< 1\%$ of the total flux, a situation that contrasts sharply, for example, with the case of Cyg X-1 where the Compton component is always unfavorably high

[1] National Astronomical Observatories, Chinese Academy of Sciences, Beijing 100012, China
[2] University of Chinese Academy of Sciences, Beijing 100012, China
[3] Harvard-Smithsonian Center for Astrophysics, 60 Garden Street, Cambridge, MA 02138, USA
[4] Department of Astronomy, San Diego State University, 5500 Campanile Drive, San Diego, CA 92182, USA
[5] Department of Astronomy, Key Laboratory of Astroparticle Physics of Yunnan Province, Yunnan University, Kunming, 650091, China

[6] Spin is usually expressed in terms of the dimensionless black-hole spin parameter $a_* = cJ/GM^2$, where a_* is subject to the Kerr bound $|a_*| < 1$, and J and M are respectively the angular momentum and mass of the black hole.

($> 10\%$; Gou et al. 2011, 2014). For NovaMus, we analyze 15 spectra, four of which we refer to as our "gold" spectra because their Compton component is minuscule, contributing $< 0.05\%$ of the total emission. In this circumstance, how one chooses to model the nonthermal component of emission is completely irrelevant, the analysis is simple and the results are particularly robust. Our estimate of spin for NovaMus is based entirely on our analysis of these four gold spectra, a result we confirm by analyzing the remaining eleven "silver" spectra whose Compton component is in the range 0.3% to 9%.

The paper is organized as follows. We discuss our data selection and their reduction in Section 2. In Section 3 we describe our methods of data analysis and present our results, first for the four gold spectra, and then for the complete sample of 15 spectra. Sections 4 and 5 are devoted respectively to a comprehensive error analysis of the four gold spectra, and then to the complete sample of 15 spectra. In Section 6 we discuss and summarize our results.

2. DATA SELECTION & REDUCTION

The X-ray data we consider for NovaMus are those presented in Ebisawa et al. (1994; hereafter EB94), which were obtained using the Large Area Counter (LAC) onboard the Japanese X-ray astronomy satellite *Ginga*. The LAC was comprised of eight identical proportional counter detectors with a total effective area of 4000 cm^2 covering the energy range from 2.0 keV to 37 keV.

We have strictly followed the procedures described in the manual *ABC Guide to the Ginga Data Analysis*[7]. The data were first cleaned and then the spectra were extracted using the software package ISAS. Among the three methods of extracting the spectra – the Simple Method, the SUD-sort Method and the Hayashida Method – we chose the latter mainly because the approach is straightforward. Hayashida et al. (1989) developed an accurate model of the background that reproduces the background rate for each energy channel, thereby making it unnecessary to extract separate background spectra. This approach is particularly well-suited in the case of a bright source like NovaMus, which reached a peak 1–6 keV X-ray intensity of ~ 8 Crab (Kitamoto et al. 1992). The extracted spectra were saved in ASCII format and (in order to be compatible with XSPEC) were converted to FITS format using the ftool *lac2xspec*, which was also used to calculate the relevant response files. As customary, we added a 2% systematic error in each channel in quadrature with the statistical error. In addition, we binned the spectra to contain at least 25 counts per channel to insure the validity of the χ^2 statistic.

Because the continuum-fitting method relies on an accurate estimate of luminosity, we corrected the effective area of the LAC using the spectrum of the Crab Nebula as a standard source by the method described in Steiner et al. (2010). Specifically, we analyzed one LAC spectrum of the Crab obtained near the time of the observations in question; compared the fit parameters obtained to those of our reference Crab spectrum of Toor & Seward (1974; $\Gamma = 2.1$ and $N = 9.7$ photons s^{-1} cm^{-2} keV^{-1}); and computed a pair of correction factors: a normalization correction, C_{TS} = 1.164$\pm$0.024 (the ratio of the fitted normalization to that of Toor & Seward) and a correction to the slope of the power-law, $\Delta\Gamma_{TS}$ = 0.022$\pm$0.009 (the difference between the observed value of the power-law index and that of Toor & Seward). These corrections were applied in all of our analysis work to each spectrum using the customized XSPEC multiplicative model CRABCOR.

[7] www.darts.isas.jaxa.jp/astro/ginga/analysis.html

3. DATA ANALYSIS AND RESULTS

Twenty-one spectra were extracted initially (see Table 1). However, six were rejected: three (Nos. 5, 15 and 16) because of their short exposure times (< 100 s) and three others (Nos. 17, 19 and 20) because their Eddington-scaled luminosities are $< 2\%$. Table 2 lists our final sample of 15 time-ordered spectra with the four gold spectra (SP1 – SP4) listed first, followed by the 11 silver spectra (SP5 – SP15). The errors considered in this section are those due solely to counting statistics. The dominant errors due to the uncertainties in the input parameters M, i, D and N_{H} are considered in the following two sections.

All data analysis and model fits were performed using XSPEC version 12.8.2 (Arnaud 1996). The spectra were fitted over the energy range 2.0 – 25.0 keV. Because of the detector's limited low-energy response, we were unable to fit for the hydrogen column density N_{H}. We estimate this parameter using two published measurements of reddening, which are consistent within 0.25σ: E(B-V) = 0.287 ± 0.004 (Cheng et al. 1992) and 0.30 ± 0.05 (Shrader & Gonzalez-Riestra 1993). Adopting this latter value and its uncertainty, and assuming $A_{\mathrm{V}}/E(B-V) = 3.1$ and $N_{\mathrm{H}}/A_{\mathrm{V}} = (2.21 \pm 0.09) \times 10^{21}$ $\mathrm{mag}^{-1}\mathrm{cm}^{-2}$ (Güver & Özel 2009), we estimate the column density to be $N_{\mathrm{H}} = (0.206 \pm 0.035) \times 10^{22}$ cm^{-2}. Throughout the paper, we use this value of N_{H} and the photoelectric absorption model TBABS with the abundances set using the command *abund wilm* (Wilms et al. 2000).

As in our earlier work on black hole spin (e.g., Gou et al. 2009, 2010), before embarking on the relativistic analysis we performed a preliminary nonrelativistic analysis of the spectra as a check that we have extracted them properly. To this end, for NovaMus we compare our results to those of EB94. Our model is TBABS$*$CRABCOR$*$(SIMPL$\otimes$DISKBB). The convolution model SIMPL is an empirical model of Comptonization with two fit parameters, the familiar photon index Γ and the scattering fraction – the fraction f_{SC} of the seed photons that are scattered into the power-law tail – which is a straightforward measure of the strength of the Compton component (Steiner et al. 2009b). We use the same nonrelativistic thin-disk model as EB94, namely DISKBB. In Table 3, we give for each of the 15 spectra our estimate of the inner disk temperature T_1 and compare our values to those obtained by EB94 (denoted in the table as T_2). Our results are consistent with those of EB94 to within about 4%. It is likely that the small differences in temperature result from using different models for the Compton component: We used SIMPL and EB94 used POWERLAW. Support for this view is provided by the four gold spectra (SP1 – SP4), which are essentially uncontaminated by power-law emission; for these spectra, the temperature differences are $< 1\%$.

Now, we turn to the relativistic analysis of our four gold spectra. Replacing DISKBB by our workhorse relativistic disk model KERRBB2, our complete model becomes:

TBABS$*$CRABCOR$*$(SIMPL$\otimes$KERRBB2)

The components TBABS, CRABCOR and SIMPL are described above. The key component of the model is KER-

RBB2, a thin accretion-disk model that includes all relativistic effects, self-irradiation of the disk, limb darkening and the effects of spectral hardening (Li et al. 2005; McClintock et al. 2014). The two fit parameters of KERRBB2 are the spin parameter a_* and the mass accretion rate $\dot{M}$. The effect of spectral hardening is incorporated into the parent model KERRBB via a pair of look-up tables for the hardening factor f corresponding to two representative values of the viscosity parameter: $\alpha = 0.01$ and 0.1. The entries in the table were computed using a second relativistic disk model BHSPEC (Davis et al. 2005; Davis & Hubeny 2006). In fitting, we turned on the effects of self-irradiation of the disk (rflag=1) and limb darkening (lflag=1).

In this section, we fix the three external input parameters at their best-fit values: $M = 11.0\ M_{\odot}$, $i = 43.2$ deg and $D = 4.95$ kpc (Wu et al. 2015b). An inspection of Table 2 shows that the fits to the four gold spectra are good, the scattering fraction negligible, the luminosity $\approx 10\%$ of the Eddington limit, and *the spin parameter is very precisely determined and lies in a narrow range,* $a_* = 0.61 - 0.64$, *which is the principal result of this section.* The much larger error in the spin parameter due to uncertainties in the parameters M, i, D and $N_{\rm H}$ is considered in the following section.

We now confirm our estimate of a_* by presenting results for the silver spectra (SP5 – SP15). Although these spectra are strongly dominated by the thermal component and quite suitable for application of the continuum-fitting method, obtaining good fits requires that we add a minor reflection component. The complete model we employ is:

TBABS∗CRABCOR∗(SIMPLR⊗KERRBB2
+KERRCONV⊗(IREFLECT⊗SIMPLC)+KERRDISK).

While more complex, the model is similar to the one used in analyzing the gold spectra. The thin-disk model KERRBB2 is again decidedly the main component. The two multiplicative models out front are the same as before. Likewise, the first term in parenthesis is the same except that SIMPL has been replaced by SIMPLR, a variant of SIMPL that computes the Compton component to accommodate a nonzero reflection fraction, and that has the ability to isolate the Compton component (Steiner et al. 2011).

The second and third additive terms in parenthesis model the reprocessed emission from the disk that results from its illumination by the power-law component. The model for the illuminating power-law component itself (the term on the far right) is SIMPLC, which is equivalent to SIMPLR⊗KERRBB2 minus the unscattered thermal component. The component IREFLECT acts solely on the power-law component to generate the reflection continuum with absorption edges; key parameters of IREFLECT are the disk ionization parameter ξ and the disk temperature T (which we fix to the value T_1 in Table 3). To complete the model of the reflected component, we follow (Brenneman & Reynolds 2006) and employ the line model KERRDISK and the convolution smearing model KERRCONV, both of which treat a_* as a free fit parameter. These models allow the emissivity indices to differ in the inner and outer regions of the disk. For simplicity, and because this parameter is unknown with values that vary widely from application to application, we use an unbroken emissivity profile with a single index q. We tie together all the common parameters of KERRDISK and KERRCONV, including the two principal parameters, namely, a_* and q. The key parameters of KERRDISK are the rest-frame line energy $E_{\rm L}$ and the photon flux in the line $N_{\rm L}$. At the level of detail, we set the inclination to our measured value of 43.2 deg; fixed the abundances of all the elements to solar; set the scaling factor in SIMPLR to -1; allowed the ionization parameter to vary; set the emissivity index to 3 in KERRCONV; and for KERRDISK adopted an unbroken emmisivity profile with a single index q while linking the spin parameter of this component to that in KERRBB2. The fitting results to the reflection components for SP5 – SP15 are listed separately in Table 4.

An inspection of Table 2 shows that the spin parameter for the eleven silver spectra is quite precisely determined. However, its value ranges rather widely from 0.47 to 0.72, while its average value is $a_* = 0.58 \pm 0.02$ (std. dev.), which is in good agreement with the value found for the gold spectra. The luminosity for the silver spectra likewise ranges widely, from 3% to 20% of the Eddington limit.

The results given in Table 2 for all 15 spectra are for our baseline value of the viscosity parameter, $\alpha = 0.1$. For our other fiducial value, $\alpha = 0.01$, the spin increases slightly and systematically, as we show in Section 4, and as we have found to be consistently the case in measuring the spins of other black holes. We assume throughout the paper that the metallicity of the disk gas is solar, although this parameter has a negligible effect on our results (e.g., see Gou et al. 2010).

One of the parameters of the reflection model IREFLECT is the disk temperature, which we fix to T_1 (Table 3). Because our T_1 differs slightly from EB94's T_2, and also because DISKBB overestimates the temperature by $\sim 5\%$ (Zimmerman et al. 2005), we test the effect on the spin parameter of increasing or decreasing the disk temperature by a factor of 2. As the three rightmost columns in Table 3 show, even such gross changes in disk temperature have a negligible effect ($< 0.5\%$) on the spin parameter.

4. COMPREHENSIVE ERROR ANALYSIS: GOLD SPECTRA

We now estimate the error in a_* resulting from the uncertainties in the input parameters M, i, D and $N_{\rm H}$, which dominate the error budget (including uncertainties in the model) in measuring spin via the continuum-fitting method (see McClintock et al. 2014; and references therein). We first quantitatively explore for each parameter separately the effect of its uncertainty on the fitted value of the spin parameter. Then, for the four gold spectra we describe our standard Monte Carlo (MC) error analysis and present our adopted final results. We perform our MC analysis on each spectrum separately, which is our usual approach, and we also fit the four gold spectra jointly.

4.1. *Effect of Varying the Input Parameters Individually*

In turn, we fixed three of the input parameters M, i, D and $N_{\rm H}$ and varied the fourth in order to assess its effect on the best-fit value of a_*. The results, which are shown in Figure 1, demonstrate that the value of the spin parameter is most sensitive to uncertainties in the distance, followed in succession by uncertainties in mass and inclination. As expected, the uncertainty in $N_{\rm H}$ is relatively unimportant because the column density is modest and the detector is unresponsive below 2 keV (Section 2).

4.2. *MC Error Analysis: Individual Fits*

The MC method has long been our standard approach to error analysis (Liu et al. 2008; Gou et al. 2009, 2010). Here,

we consider only the four gold spectra and the effects of uncertainties in the four parameters M, i, D and $N_{\rm H}$. In our analysis, we assumed that $N_{\rm H}$ is Gaussian distributed, and we used the log-normal function to describe the asymmetric distributions of the parameters M, i, and D. We first fixed the viscosity parameter to our baseline value, $\alpha = 0.1$. Following the prescription described in Gou et al. (2009, 2010), for each of the four spectra (SP1–SP4 in Table 2) we (1) generated 3000 sets of the four parameters assuming that they are independent and normally distributed; (2) computed for each set of input parameters the KERRBB2 look-up table for the spectral hardening factor f; and (3) fitted the spectrum to determine a_*.

We then performed the MC analysis for $\alpha = 0.01$ following precisely the same procedures. The resultant histograms for $\alpha = 0.01$ and $\alpha = 0.1$ showing the number of occurrences vs. the spin parameter, and a summation of the two histograms, are presented in Figure 2 by a dashed line, a thin solid line and a thick solid line, respectively. Clearly, the effect of varying the viscosity parameter is slight. Adopting the summed histogram, *we arrive at our final adopted estimate of the spin parameter:* $a_* = 0.63^{+0.16}_{-0.19}$ (1σ level of confidence). Uncertainty ranges at three other levels of confidence are summarised in Table 5. The effect on the spin parameter of varying individually the four input parameters is illustrated in Figure 3.

4.3. *MC Error Analysis: Joint Fit*

We now show that the alternative approach of fitting the four gold spectra simultaneously produces results that are essentially identical to our adopted results (which were obtained by fitting the spectra individually). In this case, we allowed all of the parameters to vary freely except the parameter of interest, namely, the spin parameter, which has a unique physical value. Repeating the MC analysis using exactly the same procedures described above, we arrived at precisely the same estimate of spin as before at the 1σ level of confidence: $a_* = 0.63^{+0.16}_{-0.19}$. Meanwhile, as summarized in the rightmost column of Table 5, the uncertainty ranges at other levels of confidence differ very slightly from our adopted results.

5. COMPREHENSIVE ERROR ANALYSIS: COMPLETE SAMPLE OF 15 SPECTRA

In order to confirm our prime result for the four gold spectra, we performed an MC error analysis on our complete sample of 15 spectra employing exactly the same procedures described in Section 4.2. The spectra were analyzed individually. Their histograms are shown in Figure 4. The final result is the summed histogram in Figure 5 plotted as a heavy solid line, which is to be compared directly to its counterpart histogram in Figure 2. In this case, the uncertainty in the spin parameter is slightly less, but the central value is essentially unchanged, which confirms our adopted result for the four gold spectra. Figure 6 (like Figure 3 for the gold spectra) shows the effect on the spin parameter of varying individually the four input parameters.

6. DISCUSSION AND CONCLUSIONS

Based on a sample of four sources, Narayan & McClintock (2012; hereafter NM12) proposed a relationship between jet power and black hole spin that is consistent with the prediction of the B-Z jet model (Blandford & Znajek 1977). Steiner et al. (2013) confirmed the relation with a fifth source and used the NM12 model to predict the spins for an additional six black holes including NovaMus. The expression for the dimensionless jet power is:

$$P_{\rm jet} = \left(\frac{\nu}{5\ {\rm GHz}}\right)\ \left(\frac{S^{\rm tot}_{\nu,0}}{\rm Jy}\right)\ \left(\frac{D}{\rm kpc}\right)^2\ \left(\frac{M}{M_\odot}\right)^{-1}, \quad (1)$$

where $S^{\rm tot}_{\nu,0}$ is the beaming-corrected flux,

$$S^{\rm tot}_{\nu,0} = S_{\nu,{\rm obs}} \times \delta^{k-3}, \quad (2)$$

ν is the observing frequency, D the distance, M the black hole mass, and δ the beaming correction factor. The parameter k is the radio spectral index whose value for NovaMus is 0.5 (Ball et al. 1995). For the approaching and receding jets, $\delta = (\Gamma(1-\beta\cos i))^{-1}$ and $\delta = (\Gamma(1+\beta\cos i))^{-1}$, respectively (Mirabel & Rodríguez 1999).

Figure 7 is a revised version of Figure 1 from Steiner et al. (2013) that shows jet power vs. spin for two typical values of Γ. Ignoring the point for NovaMus (red open square), the difference between our figure and the one of Steiner et al. is that we use for GRS 1915+105 new estimates of the key parameters: $M = 12.4\ M_\odot, D = 8.6$ kpc, $i = 60$ deg and $a_* = 0.98^{+0.01}_{-0.02}$ (Reid et al. 2014). Using these data and the relations above, we re-estimated the jet power for GRS 1915+105 and updated the corresponding data point in Figure 7. We then re-fitted the data for the five sources (blue filled circles) using the least χ^2 method; the resultant relation describing the model curves in Figure 7 is:

$$P_{\rm jet} = \left(\frac{a_*}{1+\sqrt{1-{a_*}^2}}\right)^2\ {\rm Jy} \times \begin{cases} {\rm Exp}(3.9\pm0.5) & (\Gamma=2) \\ {\rm Exp}(6.9\pm0.5) & (\Gamma=5). \end{cases}$$

In estimating the jet power of NovaMus, for the 5 GHz flux we use values that range from 0.2 Jy to 1.0 Jy (see Footnote 1 of Table 1 in Steiner et al. 2013), which we take to be a 1σ range. As the central value, we adopt the geometric mean of these two values, namely 0.45 Jy. The flux is therefore $S_{\nu,{\rm obs}} = 0.45^{+0.55}_{-0.25}$ Jy or, equivalently, $\log(S_{\nu,{\rm obs}}/{\rm Jy}) = -0.35 \pm 0.35$. Using the equations above, the corresponding values of jet power are $0.35^{+0.43}_{-0.19}$ for $\Gamma = 2$ and $3.5^{+4.3}_{-1.9}$ for $\Gamma = 5$. Using these estimates of jet power and our MC estimate of spin for NovaMus, we added a sixth data point to Figure 7. Considering the uncertainties in both the model and the data, the point for NovaMus lies off the model curves by 1.9σ for $\Gamma = 2$ and 2.1σ for $\Gamma = 5$.

Morningstar et al. (2014; M14) reported a retrograde spin for the black hole in NovaMus: $a_* = -0.25^{+0.05}_{-0.64}$ (90% confidence level). As discussed in detail by Fragos & McClintock (2015), this is a surprising result. In contrast, we find a moderately high value of spin, $a_* = 0.63^{+0.16}_{-0.19}$, and rule strongly against a retrograde value: $a_* > 0.17$ (2σ or 95.4% confidence level).

We and M14 analyzed the same *Ginga* X-ray data and we both used the continuum-fitting method. Ignoring the crudeness of M14's error analysis and treatment of spectral hardening, the crucial difference between our study and theirs is the choice of the key input parameters: The values they gleaned from the literature were $M = 7.24 \pm 0.07\ M_\odot$, $i = 54 \pm 1.5$ deg, and $D = 5.89 \pm 0.26$ kpc. Meantime, our adopted values are $M = 11.0^{+2.1}_{-1.4}\ M_\odot$, i $= 43.2^{+2.1}_{-2.7}$ deg, $D = 4.95^{+0.69}_{-0.65}$ kpc (Wu et al. 2015b). As Figure 1 makes clear, each of M14's input parameters *considered individually* –

specifically, their 50% lower mass, 10.8 deg higher inclination and 16% greater distance – is responsible for driving their spin estimate downward, and for their conclusion that the spin is retrograde. The principal reference they cite for the values of M, i and D they adopt is a one-page conference paper (Gelino 2004), which in turn is based on Gelino et al. (2001). This latter paper, which arrives at an inflated estimate of the inclination, and hence low value for the mass, is based on a flawed analysis of the ellipsoidal light curves that ignores a substantial contribution of light from the accretion disk (see Sections 3 and 5 in Wu et al. 2015a).

The X-ray data we have used in estimating the spin of NovaMus via the continuum-fitting method are of extraordinary quality. In particular, despite the excellent performance of the *Ginga* LAC detectors at high energies, the four gold spectra show essentially no evidence of a power-law component. These pure thermal spectra, which are ideal for application of the continuum-fitting method, our accurate estimates of M, i and D, and the demonstrated robustness of the continuum-fitting method provide a firm estimate of the spin of the black hole in NovaMus: $a_* = 0.63^{+0.16}_{-0.19}$. This result is confirmed by our analysis of eleven additional spectra of lower quality.

REFERENCES

Arnaud, K. A. 1996, in Astronomical Society of the Pacific Conference Series, Vol. 101, Astronomical Data Analysis Software and Systems V, ed. G. H. Jacoby & J. Barnes, 17
Ball, L., Kesteven, M. J., Campbell-Wilson, D., Turtle, A. J., & Hjellming, R. M. 1995, MNRAS, 273, 722
Blandford, R. D. & Znajek, R. L. 1977, MNRAS, 179, 433
Brandt, S., Castro-Tirado, A. J., Lund, N., Dremin, V., Lapshov, I., & Sunyaev, R. 1992, A&A, 254, L39
Brenneman, L. W. & Reynolds, C. S. 2006, ApJ, 652, 1028
Cheng, F. H., Horne, K., Panagia, N., Shrader, C. R., Gilmozzi, R., Paresce, F., & Lund, N. 1992, ApJ, 397, 664
Davis, S. W., Blaes, O. M., Hubeny, I., & Turner, N. J. 2005, ApJ, 621, 372
Davis, S. W. & Hubeny, I. 2006, ApJS, 164, 530
Ebisawa, K. et al. 1994, PASJ, 46, 375
Fabian, A. C., Rees, M. J., Stella, L., & White, N. E. 1989, MNRAS, 238, 729
Fragos, T. & McClintock, J. E. 2015, ApJ, 800, 17
Fragos, T., Tremmel, M., Rantsiou, E., & Belczynski, K. 2010, ApJ, 719, L79
Gelino, D. M. 2004, in Revista Mexicana de Astronomia y Astrofisica, vol. 27, Vol. 20, Revista Mexicana de Astronomia y Astrofisica Conference Series, ed. G. Tovmassian & E. Sion, 214–214
Gelino, D. M., Harrison, T. E., & McNamara, B. J. 2001, AJ, 122, 971
Gou, L. et al. 2009, ApJ, 701, 1076
— 2011, ApJ, 742, 85
— 2014, ApJ, 790, 29
Gou, L., McClintock, J. E., Steiner, J. F., Narayan, R., Cantrell, A. G., Bailyn, C. D., & Orosz, J. A. 2010, ApJ, 718, L122
Güver, T. & Özel, F. 2009, MNRAS, 400, 2050
Hayashida, K., Inoue, H., Koyama, K., Awaki, H., & Takano, S. 1989, PASJ, 41, 373
Kitamoto, S., Tsunemi, H., Miyamoto, S., & Hayashida, K. 1992, ApJ, 394, 609
Kulkarni, A. K. et al. 2011, MNRAS, 414, 1183
Li, L.-X., Zimmerman, E. R., Narayan, R., & McClintock, J. E. 2005, ApJS, 157, 335
Liu, J., McClintock, J. E., Narayan, R., Davis, S. W., & Orosz, J. A. 2008, ApJ, 679, L37
McClintock, J. E., Narayan, R., & Steiner, J. F. 2014, Space Sci. Rev., 183, 295
McClintock, J. E., Shafee, R., Narayan, R., Remillard, R. A., Davis, S. W., & Li, L.-X. 2006, ApJ, 652, 518
Mirabel, I. F. & Rodríguez, L. F. 1999, ARA&A, 37, 409
Morningstar, W. R., Miller, J. M., Reis, R. C., & Ebisawa, K. 2014, ApJ, 784, L18
Narayan, R. & McClintock, J. E. 2012, MNRAS, 419, L69
Noble, S. C., Krolik, J. H., Schnittman, J. D., & Hawley, J. F. 2011, ApJ, 743, 115
Penna, R. F., McKinney, J. C., Narayan, R., Tchekhovskoy, A., Shafee, R., & McClintock, J. E. 2010, MNRAS, 408, 752
Reid, M. J., McClintock, J. E., Steiner, J. F., Steeghs, D., Remillard, R. A., Dhawan, V., & Narayan, R. 2014, ApJ, 796, 2
Remillard, R. A., McClintock, J. E., & Bailyn, C. D. 1992, ApJ, 399, L145
Reynolds, C. S. 2014, Space Sci. Rev., 183, 277
Shafee, R., McKinney, J. C., Narayan, R., Tchekhovskoy, A., Gammie, C. F., & McClintock, J. E. 2008, ApJ, 687, L25
Shrader, C. R. & Gonzalez-Riestra, R. 1993, A&A, 276, 373
Steiner, J. F. & McClintock, J. E. 2012, ApJ, 745, 136
Steiner, J. F., McClintock, J. E., & Narayan, R. 2013, ApJ, 762, 104
Steiner, J. F., McClintock, J. E., Orosz, J. A., Remillard, R. A., Bailyn, C. D., Kolehmainen, M., & Straub, O. 2014, ApJ, 793, L29
Steiner, J. F., McClintock, J. E., Remillard, R. A., Gou, L., Yamada, S., & Narayan, R. 2010, ApJ, 718, L117
Steiner, J. F., McClintock, J. E., Remillard, R. A., Narayan, R., & Gou, L. 2009a, ApJ, 701, L83
Steiner, J. F., Narayan, R., McClintock, J. E., & Ebisawa, K. 2009b, PASP, 121, 1279
Steiner, J. F. et al. 2011, MNRAS, 416, 941
Toor, A. & Seward, F. D. 1974, AJ, 79, 995
Wilms, J., Allen, A., & McCray, R. 2000, ApJ, 542, 914
Wu, J., Orosz, J. A., McClintock, J. E., Gou, L., Bailyn, C. D., & Hasan, I. 2015b, to be submitted
Wu, J. et al. 2015a, ApJ, 806, 92
Zhang, S. N., Cui, W., & Chen, W. 1997, ApJ, 482, L155
Zhu, Y., Davis, S. W., Narayan, R., Kulkarni, A. K., Penna, R. F., & McClintock, J. E. 2012, MNRAS, 424, 2504
Zimmerman, E. R., Narayan, R., McClintock, J. E., & Miller, J. M. 2005, ApJ, 618, 832

Table 1
Ginga X-ray Observations of Nova Muscae 1991

N	Time (1991 UT)	Exposure Time (seconds)	Counts	$L/L_{\rm Edd}$
1	$2/13$ $5:06-5:23$	391	10265400	0.201
2	$2/13$ $6:40-6:57$	412	10236100	0.197
3	$2/13$ $8:14-8:34$	598	14826300	0.196
4	$2/14$ $4:36-4:53$	219	5208070	0.189
5	$2/14$ $5:30-5:34$	31	739773	0.191
6	$2/20$ $23:31-23:37$	83	1619840	0.163
7	$2/21$ $0:23-0:30$	166	3212070	0.162
8	$3/08$ $18:04-18:22$	472	5285530	0.103
9	$3/10$ $16:56-17:17$	321	3303930	0.093
10	$3/20$ $12:56-13:17$	532	5175480	0.090
11	$3/28$ $9:37-9:43$	140	1607220	0.103
12	$3/29$ $5:54-6:06$	457	5251350	0.104
13	$3/30$ $8:36-8:54$	655	7187840	0.099
14	$4/02$ $5:04-5:30$	934	10122400	0.099
15	$4/19$ $21:06-21:20$	31	179975	0.064
16	$5/17$ $3:12-3:20$	291	664975	0.031
17	$5/17$ $4:34-4:57$	681	1263360	0.010
18	$5/17$ $7:49-8:10$	978	2387950	0.033
19	$5/18$ $2:18-2:40$	691	1415900	0.018
20	$5/18$ $3:52-4:17$	1144	1776410	0.010
21	$5/18$ $5:25-5:52$	1330	3368750	0.031

Note. — All the spectra analyzed by EB94 with Eddington-scaled luminosities between 1% and 30% are listed here. In our analysis, we ignore six of these spectra (Nos. 5, 15, 16, 16, 19 and 20) for the reasons given in the text.

Table 2
Fit Results for Nova Muscae 1991

	N	SIMPLR		KERRBB2		χ^2_ν/d.o.f.	f	$L/L_{\rm Edd}$
		Γ	$f_{\rm SC}$	a_*	$\dot{M}$			
SP1	11	1.63 ± 0.46	0.00034 ± 0.00024	0.62 ± 0.01	1.70 ± 0.03	$1.70/23$	1.63	0.103
SP2	12	1.90 ± 0.67	0.00022 ± 0.00024	0.61 ± 0.01	1.74 ± 0.03	$0.98/24$	1.63	0.104
SP3	13	1.63 ± 0.47	0.00016 ± 0.00012	0.64 ± 0.01	1.60 ± 0.03	$0.82/27$	1.63	0.099
SP4	14	1.96 ± 0.30	0.00041 ± 0.00020	0.62 ± 0.01	1.65 ± 0.03	$1.07/28$	1.63	0.099
SP5	1	2.24 ± 0.05	0.057 ± 0.0048	0.72 ± 0.02	2.30 ± 0.08	1.14/27	1.68	0.201
SP6	2	2.11 ± 0.05	0.034 ± 0.0030	0.63 ± 0.02	2.66 ± 0.08	0.81/27	1.67	0.198
SP7	3	2.00 ± 0.04	0.026 ± 0.0022	0.65 ± 0.02	2.62 ± 0.09	1.72/27	1.67	0.198
SP8	4	2.38 ± 0.06	0.034 ± 0.0038	0.47 ± 0.03	3.32 ± 0.13	1.62/27	1.67	0.194
SP9	6	2.23 ± 0.09	0.022 ± 0.0043	0.54 ± 0.03	2.70 ± 0.12	0.45/27	1.66	0.166
SP10	7	2.39 ± 0.05	0.032 ± 0.0028	0.53 ± 0.02	2.73 ± 0.10	0.66/27	1.66	0.165
SP11	8	2.37 ± 0.38	0.004 ± 0.0037	0.55 ± 0.02	1.86 ± 0.07	0.99/27	1.63	0.104
SP12	9	2.71 ± 0.54	0.004 ± 0.0055	0.53 ± 0.02	1.73 ± 0.07	0.73/24	1.62	0.093
SP13	10	2.94 ± 0.68	0.005 ± 0.0073	0.61 ± 0.01	1.53 ± 0.04	0.94/25	1.62	0.090
SP14	18	2.35 ± 0.05	0.033 ± 0.0040	0.54 ± 0.02	0.67 ± 0.03	1.02/27	1.52	0.033
SP15	21	2.35 ± 0.04	0.066 ± 0.0063	0.62 ± 0.02	0.55 ± 0.03	0.81/27	1.52	0.032

Note. — From left to right, and for the model components indicated, the columns contain: (1) The name of the spectrum; (2) the corresponding index number from Table 1; (3) photon power-law index; (4) scattering fraction; (5) spin parameter; (6) mass accretion rate in units of 10^{18} g s^{-1}; (7) reduced chi-square and degrees of freedom; (8) spectral hardening factor; (9) bolometric Eddington-scaled X-ray luminosity of the thermal disk component. For the silver spectra SP5–SP15 (which include a reflection component modeled using IREFLECT and KERRDISK), the values of three additional fit parameters are given in Table 4.

Table 3
Influence of Disk Temperature on the Spin Parameter

	N	T(KeV)			spin		
		T_1	T_2	relative difference	$a_*(T_1)$	$a_*(2T_1)$	$a_*(0.5T_1)$
SP1	11	0.713	0.716	0.4%	–	–	–
SP2	12	0.719	0.720	0.1%	–	–	–
SP3	13	0.727	0.733	0.8%	–	–	–
SP4	14	0.720	0.716	0.5%	–	–	–
SP5	1	0.831	0.810	2.6%	0.7134	0.7143	0.7130
SP6	2	0.800	0.784	2.0%	0.6338	0.6340	0.6311
SP7	3	0.844	0.795	6.2%	0.6447	0.6443	0.6450
SP8	4	0.777	0.757	2.6%	0.5131	0.5144	0.5126
SP9	6	0.762	0.740	3.0%	0.5735	0.5735	0.5729
SP10	7	0.760	0.735	3.4%	0.5422	0.5438	0.5416
SP11	8	0.702	0.707	0.7%	0.5634	0.5633	0.5634
SP12	9	0.674	0.678	0.5%	0.5434	0.5434	0.5435
SP13	10	0.674	0.702	4.0%	0.6166	0.6165	0.6169
SP14	18	0.506	0.502	0.8%	0.5428	0.5445	0.5426
SP15	21	0.510	0.497	2.6%	0.6282	0.6302	0.6278

Note. — T_1 is our fitted value of temperature and T_2 is the value reported by EB94; N is the index number given in Table 1.

Table 4
Fit Results for the Reflection Components for the Silver Spectra

	N	KERRDISK		IREFLECT		χ^2_ν/d.o.f.	f	$L/L_{\rm Edd}$
		$E_{\rm L}$	$N_{\rm L}$	T	ξ			
SP5	1	6.97± 0.31	0.038 ± 0.008	0.83	100000 ± 249879	1.14/27	1.68	0.201
SP6	2	6.97± 0.25	0.029 ± 0.006	0.81	100000 ± 264214	0.81/27	1.67	0.198
SP7	3	6.97± 0.19	0.026 ± 0.007	0.83	100000 ± 275646	1.72/27	1.67	0.198
SP8	4	6.46± 0.35	0.009 ± 0.005	0.78	279 ± 276	1.62/27	1.67	0.194
SP9	6	6.66± 0.70	0.004 ± 0.004	0.76	1598 ± 1567	0.45/27	1.66	0.166
SP10	7	6.50± 0.39	0.006 ± 0.004	0.76	184 ± 135	0.66/27	1.66	0.165
SP11	8	6.62± 0.31	0.002 ± 0.001	0.70	749 ± 5442	0.99/27	1.63	0.104
SP12	9	6.40± 1.16	0.001 ± 0.001	0.67	1077 ± 13609	0.73/24	1.62	0.093
SP13	10	6.97± 0.58	0.001 ± 0.001	0.69	872 ± 12932	0.94/25	1.62	0.090
SP14	18	6.55± 0.26	0.001 ±0.0004	0.51	343 ± 217	1.02/27	1.52	0.033
SP15	21	6.44± 0.33	0.002 ± 0.001	0.51	390 ± 227	0.81/27	1.52	0.032

Note. — From left to right, and for the model components indicated, the columns contain: (1) The name of the spectrum; (2) the corresponding index number from Table 1; (3) the central line energy in keV limited from 6.4 to 6.97; (4) line flux in units of photons cm^{-2} s^{-1}; (5) disk temperature in keV; (6) ionization parameter in units of erg cm^{-2} s^{-1}; (7) reduced chi-square and degrees of freedom; (8) spectral hardening factor; (9) bolometric Eddington-scaled X-ray luminosity of the thermal disk component. For all spectra, we adopt the standard value of the emissivity index, $q = 3$. For spectra SP5–7, the disk ionization parameter is pegged at its maximum value, ξ=10^5 erg cm^{-2} s^{-1}.

Table 5
Spin Determinations for Different Confidence Levels

Confidence Level	Spin Interval (a_*)	
	MC Method (Adopted)	MC Method (Joint Fit)
$68.3\%(1\sigma)$	$0.63^{+0.16}_{-0.19}$	$0.63^{+0.16}_{-0.19}$
90%	$0.63^{+0.19}_{-0.25}$	$0.63^{+0.20}_{-0.24}$
$95.4\%(2\sigma)$	$0.63^{+0.26}_{-0.42}$	$0.63^{+0.26}_{-0.40}$
$99.7\%(3\sigma)$	$0.63^{+0.34}_{-0.70}$	$0.63^{+0.33}_{-0.68}$

Note. — Confidence levels for our four gold spectra SP1–SP4 resulting from our MC error analysis for both the fits to the individual spectra and for the joint fit. The results are marginalized over our two fiducial values of the viscosity parameter, $\alpha = 0.1$ and $\alpha = 0.01$.

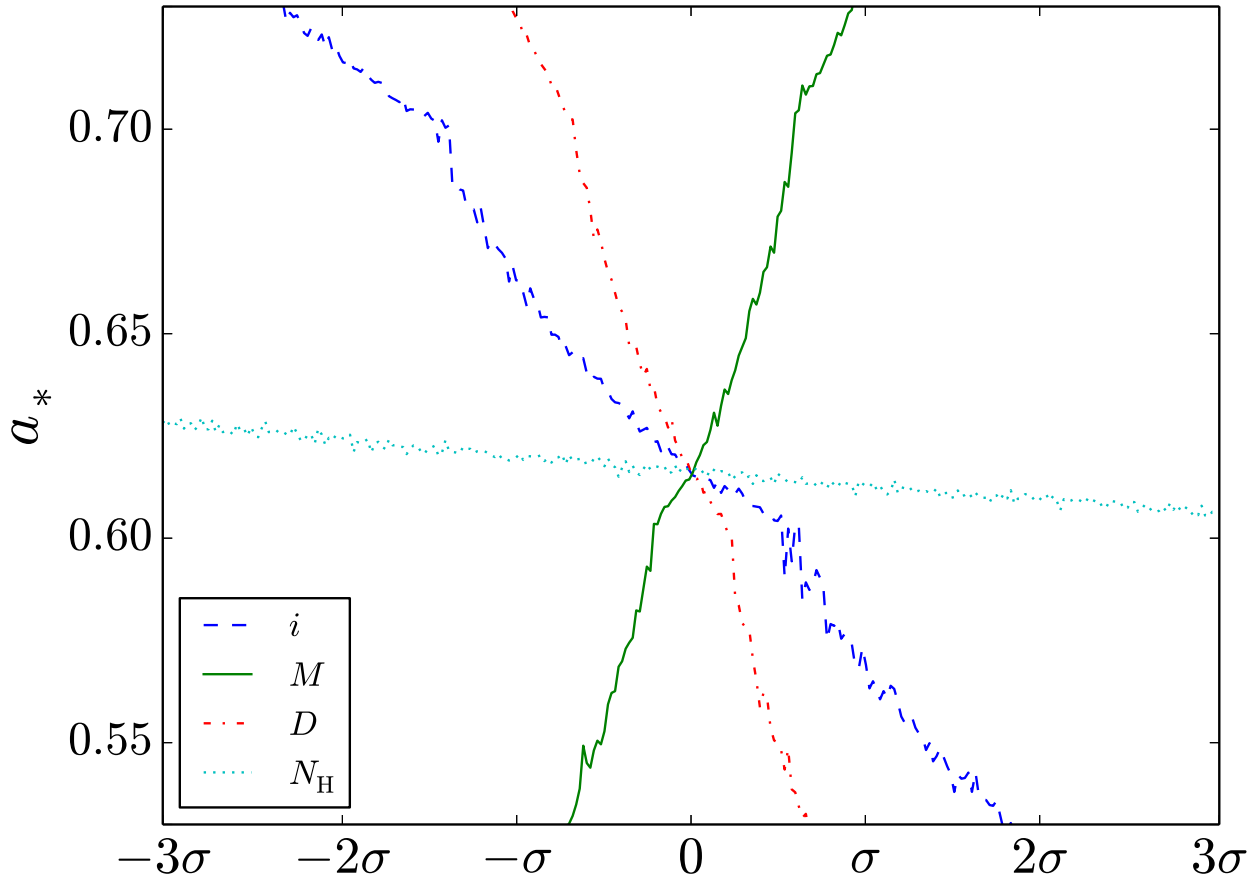

Figure 1. Dependence of the spin parameter a_* on each of the four input parameters considered individually. The difference between the value of a given parameter and its fiducial value is expressed in standard deviations. The jaggedness of the lines is an artifact of the MC sampling.

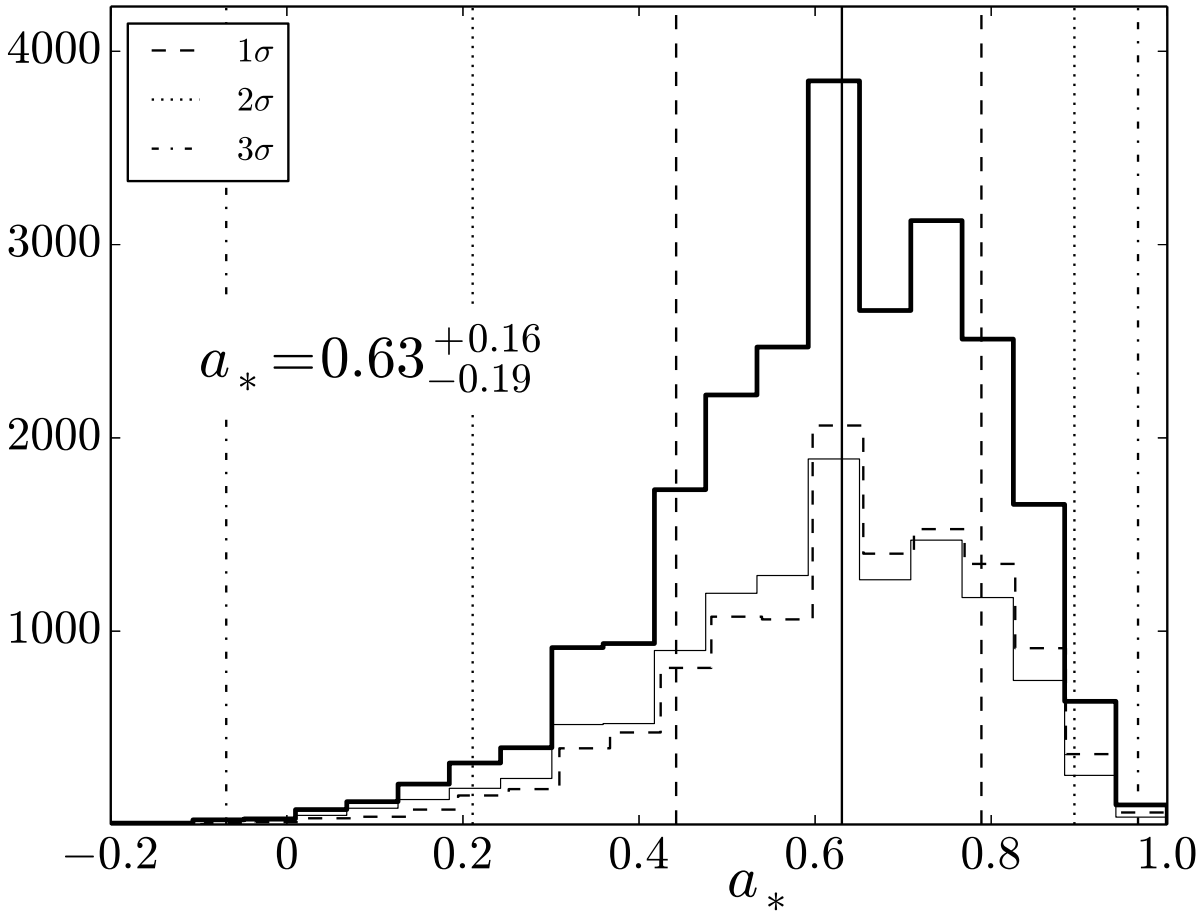

Figure 2. Histograms of the distribution of the spin parameter computed using the MC method for our gold spectra SP1–SP4 (Table 2). The histograms plotted using a thin solid line and a dashed line were computed for α = 0.1 and α= 0.01, respectively. The summation of these two histograms is shown as a bold solid line. The histograms were computed for 3000 parameter sets for each spectrum and for each of the values of the viscosity parameter, for a total of 24,000 data points. The estimate of the spin parameter given is our final, adopted value.

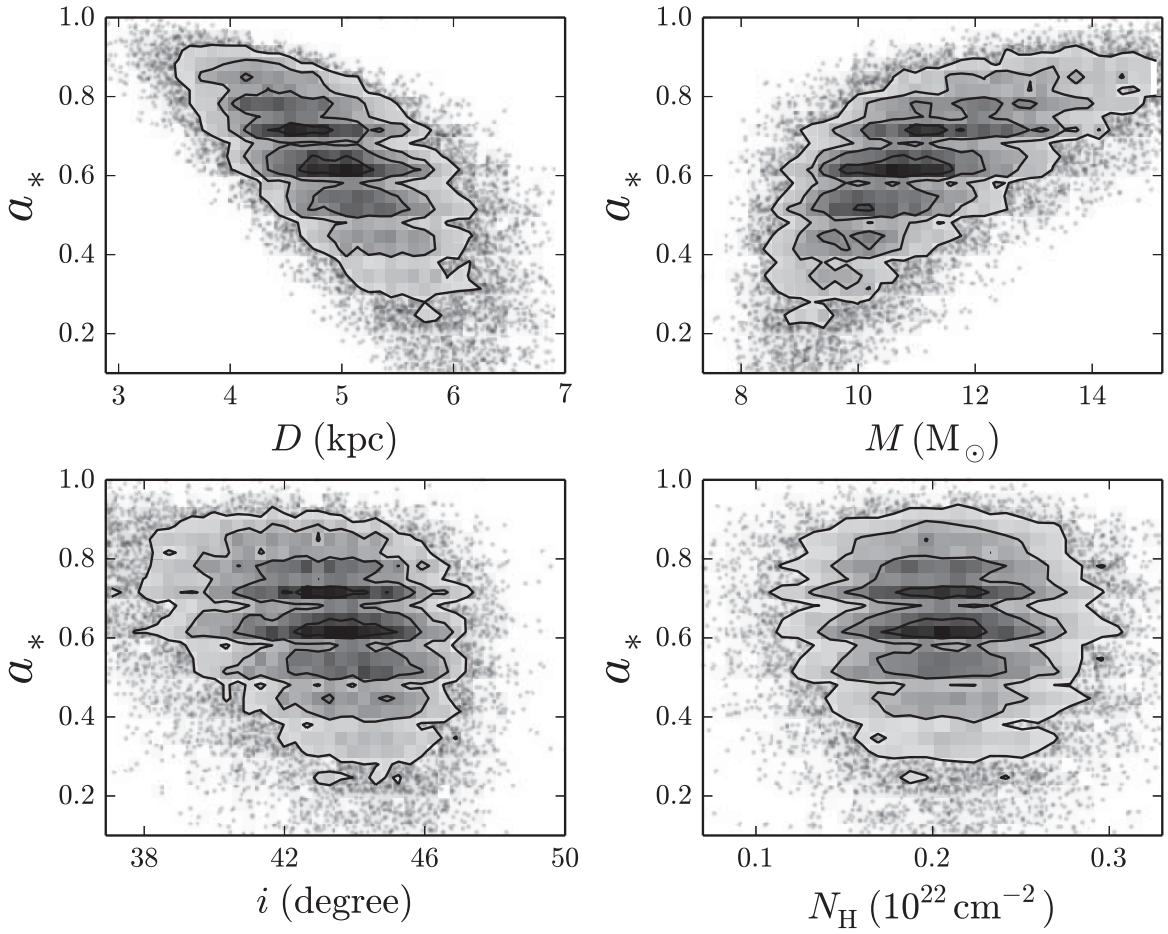

Figure 3. Correlation plots for the MC method showing the effect on the spin parameter of varying M, i, D and N_{H}, while marginalizing over our two fiducial values of the viscosity parameter. Each panel contains 24,000 data points (see Figure 2).

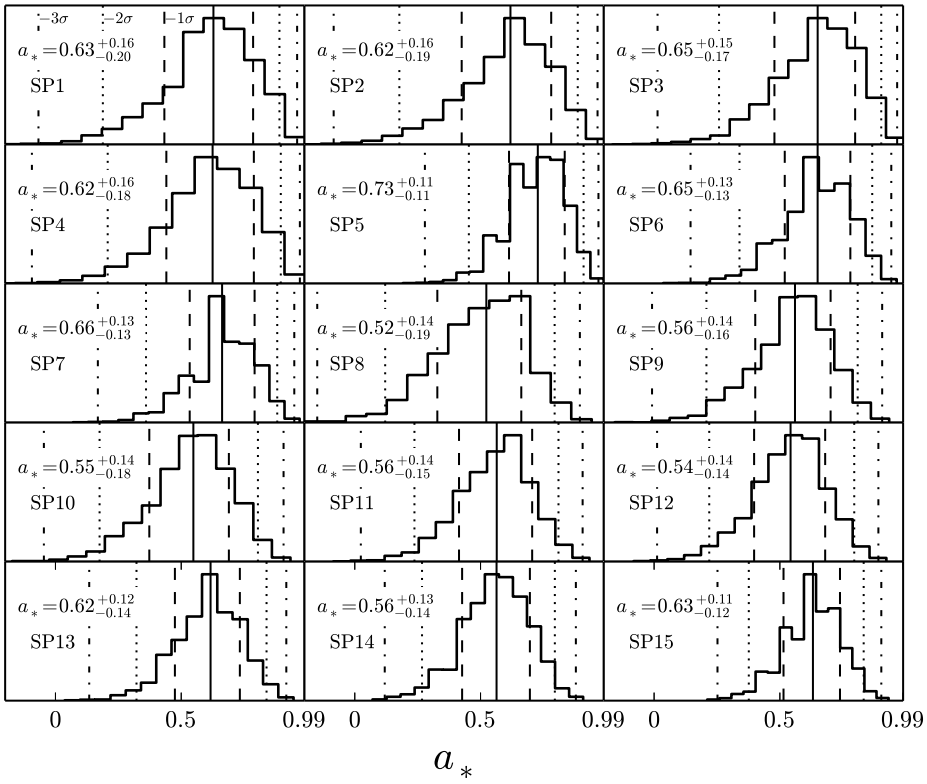

Figure 4. Results of our MC error analysis for the complete sample of 15 spectra. The histogram in each panel is a summation of a pair of histograms, one computed for $\alpha = 0.1$ and the other for $\alpha = 0.01$ (see Figure 2).

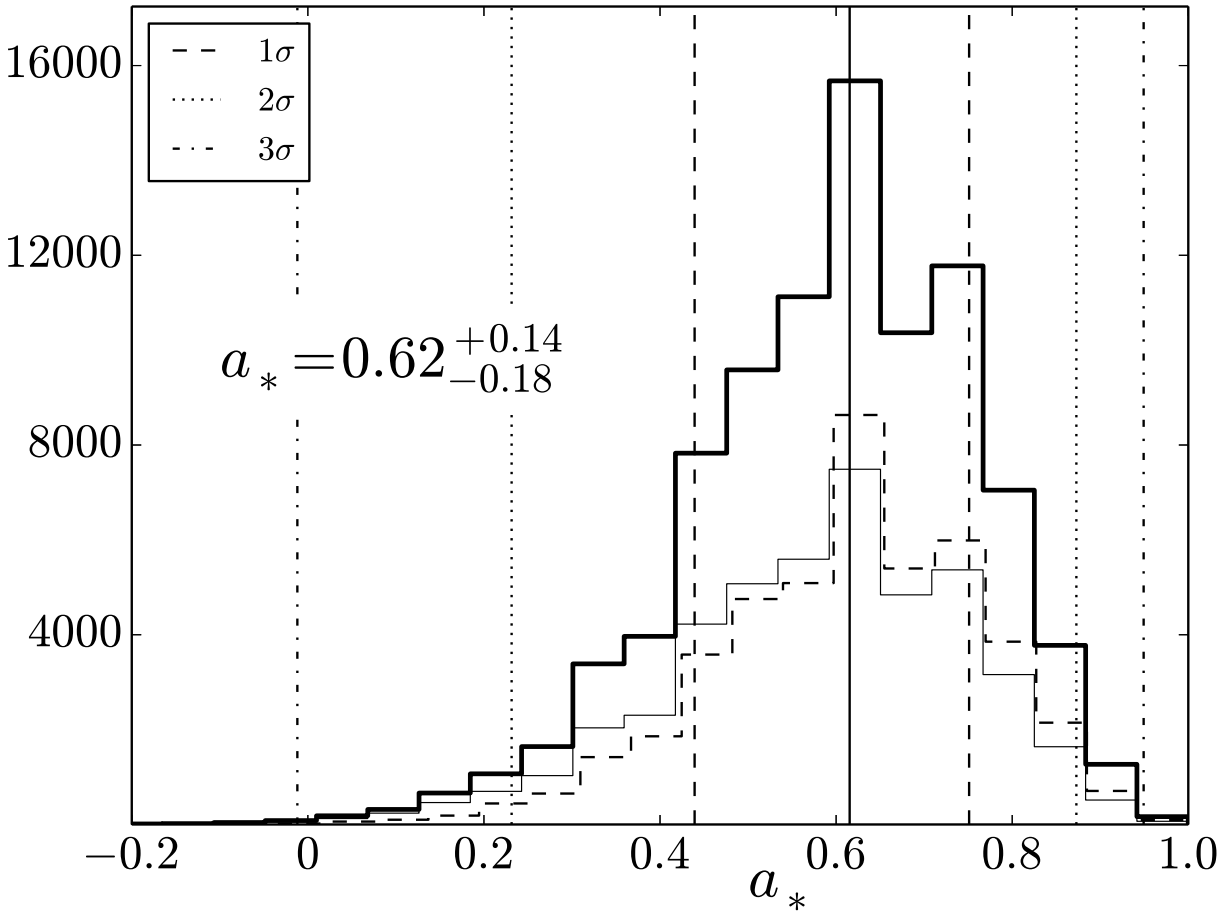

Figure 5. Histograms of the distribution of spins generated by our MC error analysis for the complete sample of 15 spectra. For a description of this figure, see Figure 2.

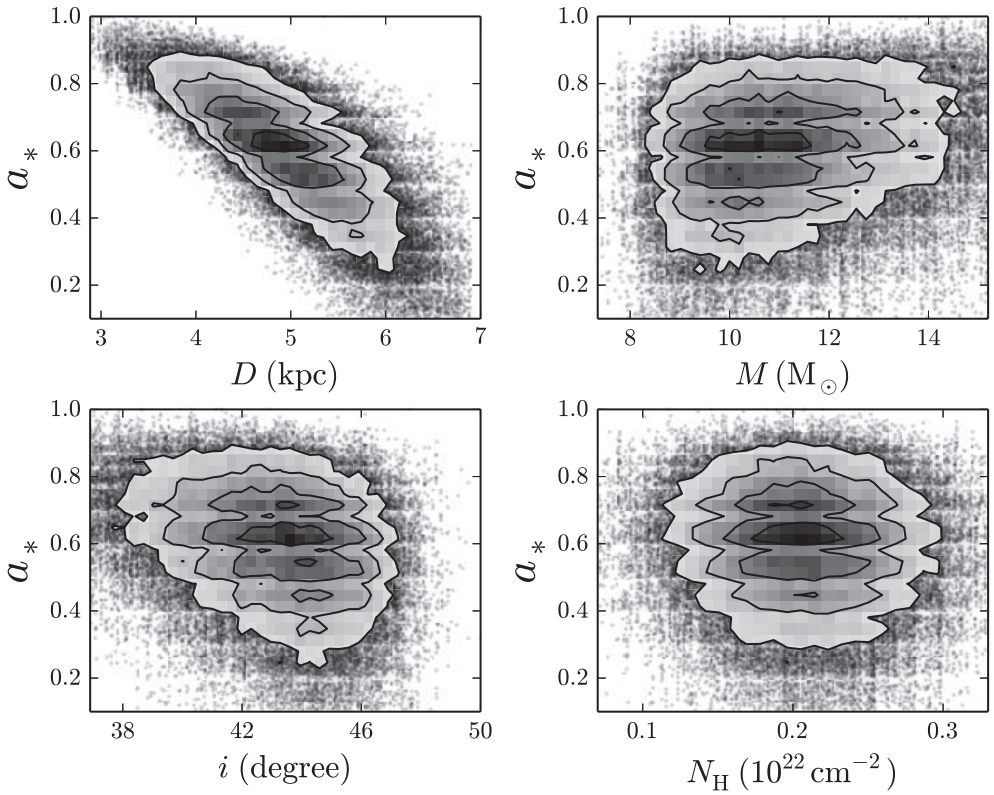

Figure 6. Same as Figure 3 for the four gold spectra except that these correlation plots result from the analysis of our complete sample of 15 spectra. In this case, each panel contains a total of 90,000 data points.

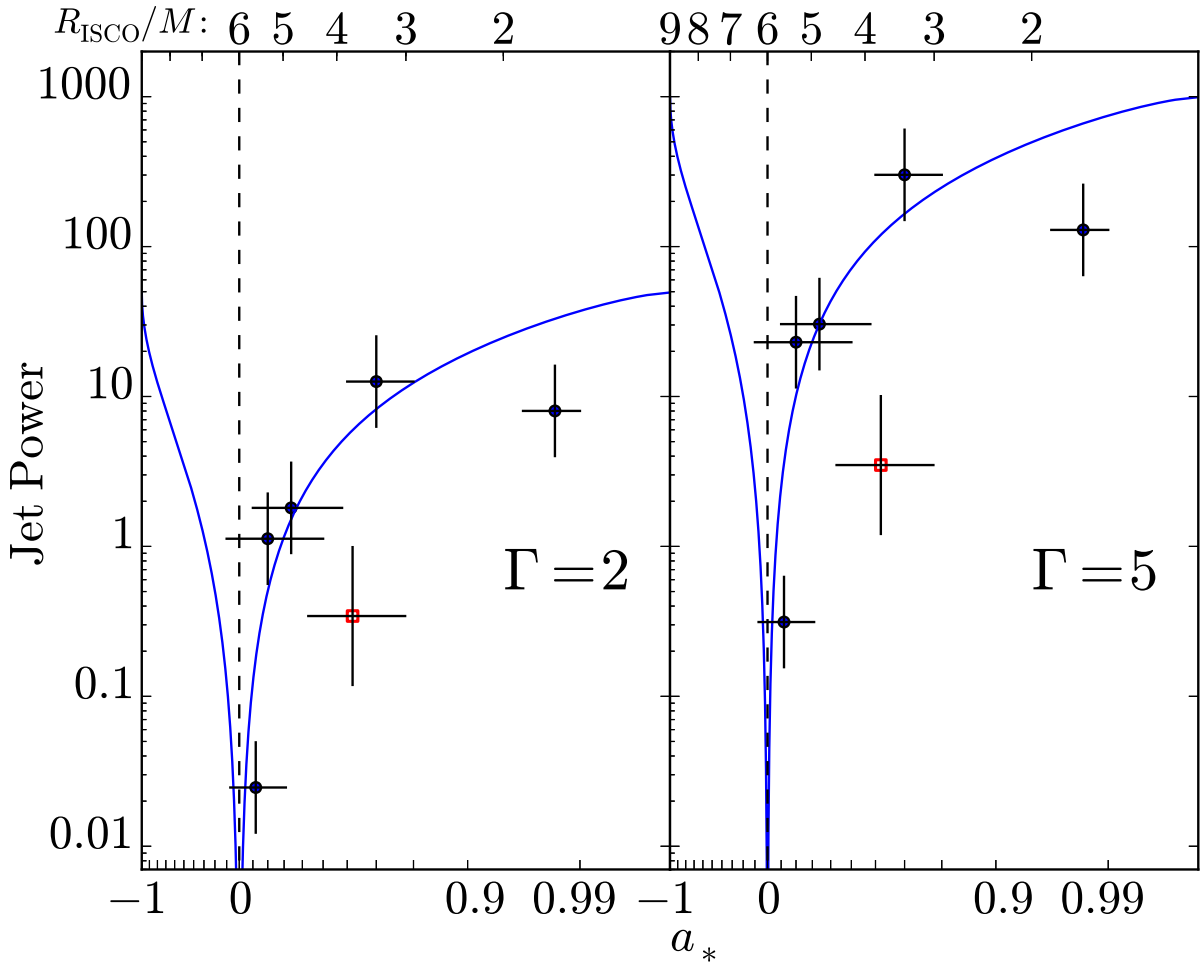

Figure 7. Relationship between radio jet power and the observable $R_{\rm ISCO}/M$ (top axis) and black hole spin (bottom axis). The curve is fitted to the five data points plotted as solid filled circles. The data point for NovaMus is plotted as an open red square.